1-2014

Effect of Er doping on the structural and magnetic properties of cobalt-ferrite

Sateesh Prathapani
University of Hyderabad, India

M. Vinitha
University of Hyderabad, India

Tanjore V. Jayaraman
University of Nebraska - Lincoln, tjayaraman2@unl.edu

D. Das
University of Hyderabad, India, ddse@uohyd.ernet.in

Effect of Er doping on the structural and magnetic properties of cobalt-ferrite

Sateesh Prathapani,[1] M. Vinitha,[1] T. V. Jayaraman,[2,a)] and D. Das[1,b)]
[1]School of Engineering Sciences and Technology, University of Hyderabad, Hyderabad 500046, India
[2]Department of Mechanical and Materials Engineering, University of Nebraska, Lincoln, Nebraska 68588, USA

(Presented 8 November 2013; received 18 September 2013; accepted 6 October 2013; published online 7 January 2014)

Nanocrystalline particulates of Er doped cobalt-ferrites $CoFe_{(2-x)}Er_xO_4$ $(0 \le x \le 0.04)$, were synthesized, using sol-gel assisted autocombustion method. Co-, Fe-, and Er- nitrates were the oxidizers, and malic acid served as a fuel and chelating agent. Calcination (400–600 °C for 4 h) of the precursor powders was followed by sintering (1000 °C for 4 h) and structural and magnetic characterization. X-ray diffraction confirmed the formation of single phase of spinel for the compositions $x = 0$, 0.01, and 0.02; and for higher compositions an additional orthoferrite phase formed along with the spinel phase. Lattice parameter of the doped cobalt-ferrites was higher than that of pure cobalt-ferrite. The observed red shift in the doped cobalt-ferrites indicates the presence of induced strain in the cobalt-ferrite matrix due to large size of the Er^{+3} compared to Fe^{+3}. Greater than two-fold increase in coercivity (~66 kA/m for $x = 0.02$) was observed in doped cobalt-ferrites compared to $CoFe_2O_4$ (~29 kA/m). © *2014 AIP Publishing LLC*. [http://dx.doi.org/10.1063/1.4854915]

Ferrimagnetic cobalt-based cubic spinels (cobalt-ferrites) possess exotic electrical and magnetic properties that are of importance in various technological applications viz. information storage systems,[1] ferro-fluid technology,[2] magnetic refrigeration,[3] magnetic diagnostics,[4] and magnetostriction.[5] In cobalt-ferrite the presence of doping elements and the thermal history during the synthesis and processing alter the metal ions distribution and hence influence their structural and magnetic properties.[6] The lanthanide series elements/ions have a net magnetic moment that depends upon the number of *f*-orbital electrons; and among them Er^{+3} is relatively small in size (89 pm), and has relatively high magnetic moment ($7\ \mu_B$).[7] The presence of Er (octahedral site of the lattice) is expected to influence the magnetic anisotropy of the doped cobalt-ferrites due to strong spin-orbit coupling. For the first time, the synthesis of nanocrystalline particulates of Er doped cobalt ferrites—$CoFe_{(2-x)}Er_xO_4$ $(0 \le x \le 0.04)$, by a sol-gel assisted autocombustion method is reported. In the present work, various concentrations of Er^{3+} are substituted in place of Fe^{3+} and their effect on the structural and magnetic properties of cobalt-ferrite was investigated.

Nanocrystalline particulates of Er doped cobalt-ferrites with nominal compositions $CoFe_{(2-x)}Er_xO_4$ (0, 0.01, 0.02, 0.03, and 0.04) were synthesized by sol-gel assisted autocombustion method. The metal precursors used were $Co(NO_3).6H_2O$, $Fe(NO_3)_3.9H_2O$ and Er_2O_3. Er_2O_3 was brought into solution, $Er(NO_3)_3xH_2O$, by mixing with HNO_3 (68%) and heating (and stirring) at 100 °C for 30 min. The metal nitrate precursors mixed with malic acid (chelating agent and fuel[8]) were subjected to heating (and stirring) at 100 °C followed by addition of ethylene glycol in 1:4 ratio (with respect to malic acid) at neutral pH, and subsequent drying led to the formation of a viscous gel. The viscous gel was transferred to an oven and maintained at 200 °C, for 3 h and it resulted in the formation of voluminous foamy precursor. The precursor was crushed into fine powders using an agate mortar and pestle and the thermo gravimetric and differential thermal analysis (TG–DTA) was performed (Mettler Toledo TGA/DSC1) at a heating rate of 10 °C/min in the range–room temperature to 1000 °C. Based on TG-DTA, the calcination temperature was identified and the precursor powders were calcined at 400–600 °C for 4 h. The calcined powders were pressed into pellets and sintered at 1000 °C for 4 h. The powder x-ray diffraction analysis (BrukerD8 Advanced–Cu K_α radiation) and the Raman spectral analysis (Lasos 77, argon laser source: $\lambda = 488$ nm and 10 mW power, and range: 200–900 cm^{-1}) was performed on the sintered samples. The magnetic characterization was performed using vibrating sample magnetometer (Lakeshore Model 7407).

Figure 1 shows the TG-DTA curves of $CoFe_{2-x}Er_xO_4$ ($x = 0.00$, 0.02, and 0.04) precursors as a representative. The curves for each of the compositions can be divided into three regions based on various processes taking place in each of them—(i) 40–150 °C, (ii) 150–400 °C, and (iii) 400–1000 °C. A similar thermal behavior was reported by Albu *et al.*, using malic acid as chelating agent.[9] In region (i)—the first step of weight loss (~10%) corresponds to the volatilization of the organic solvents and represents exothermic peak (on DTA) around 115 °C curve for $x = 0$; and the less intense endothermic peaks on DTA curve corresponds to the evaporation of the residual moisture around (85 °C) in all the compositions. In region (ii)—all the compositions show two exothermic peaks around 300 °C (DTA curve) corresponding to ~50% weight loss. These peaks are probably due to the decomposition of complex gel network $[Fe_{2-x}RE_xCo(C_4H_4O_5)(OH)_4].6H_2O$.[10] The humongous

a)Present address: Carpenter Technology Corporation, PO Box 14662, Reading, Pennsylvania 19610, USA.
b)Author to whom correspondence should be addressed. Electronic mail: ddse@uohyd.ernet.in.

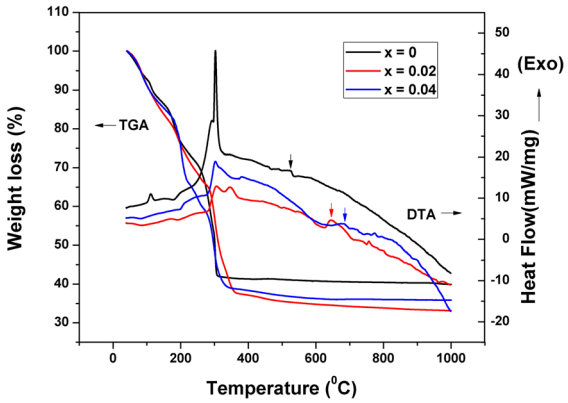

FIG. 1. The TG-DTA curves of $CoFe_{2-x}Er_xO_4$ ($x = 0.0$, 0.02, and 0.04) precursors.

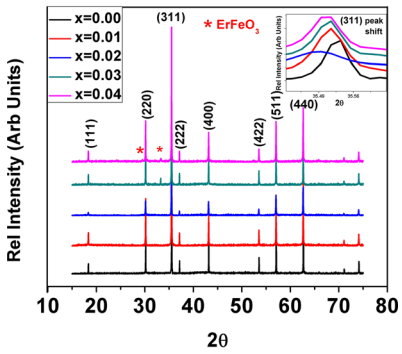

FIG. 2. X-ray diffraction spectra and (inset) (311) peak shift of $CoFe_{2-x}Er_xO4$ ($x = 0$, 0.01, 0.02, 0.03, and 0.04) sintered at 1000 °C for 4 h.

weight loss of gel network is due to the combustion reaction resulting in evolution of NH_3 and NO_2 corresponds to one of the peaks; and the other peak is likely associated with the burning of residual organic complex or oxidation of residual carbon in the gel network. In region (iii)—the peak at 535 °C for $CoFe_2O_4$ (DTA curve) shows no significant weight loss (TG curve) that can be attributed to crystallization. The crystallization is also evidenced in powder x-ray diffraction (not shown here) of calcined powders of 400 °C and 600 °C $CoFe_{2-x}Er_xO_4$ ($0 \le x \le 0.04$). To incorporate larger size Er^{3+} into the cobalt-ferrite lattice, higher energy is needed and therefore with increasing dopant concentration, some of the energy is utilized to incorporate Er^{3+} into cobalt-ferrite lattice, as a result crystallization takes place at relative higher temperatures in doped cobalt-ferrites.

Figure 2 shows the x-ray diffraction spectra for the sintered (1000 °C for 4 h) Er doped cobalt-ferrites, $CoFe_{2-x}Er_xO_4$ ($x = 0$, 0.01, 0.02, 0.03, and 0.04). The spectra show the presence of desired cubic spinel phase in all the compositions. The emergence of extraneous orthoferrite phase ($ErFeO_3$) is evident at higher Er content ($x = 0.03$ and 0.04). The lattice parameter (a) of the spinel phase was calculated by Cohen's method[11] (Table I). The a for $CoFe_2O_4$ (8.3810 ± 0.0008) is similar to a reported for cobalt-ferrite in literature and minor variation compared to literature is likely due to the variation in impurity level of the initial raw materials and method of synthesis of cobalt-ferrite.[12] Cobalt-ferrite in its inverse-spinel form has half Fe^{3+} occupying the tetrahedral site while the other half Fe^{3+} and Co^{2+} occupy the octahedral sites. Any variation in the site occupation of Fe^{3+} and Co^{2+} mostly due to synthesis method adopted is known to affect a.[13] Er^{3+} being larger in size than Fe^{3+}, its substitution increases a for $CoFe_{2-x}Er_xO_4$ ($x = 0.01$, 0.02, 0.03, and 0.04) as compared to that of $CoFe_2O_4$ (evident from the (311) peak shift–inset Figure 2). The near constant value of a for Er substituted cobalt-ferrite suggests limited solubility of Er in cubic spinel lattice, which is corroborated by the formation of $ErFeO_3$ especially at higher value of x (0.03 and 0.04). The crystallite size and strain values (using Scherrer's formula[14]) are compiled in Table I. While the crystallite size (130–160 nm) of the Er doped cobalt-ferrites were lower than pure cobalt-ferrite (~190 nm); the lattice strain of Er doped cobalt-ferrites were higher than pure cobalt-ferrite.

The formation of mixed spinel structure with various concentration of Er was confirmed by Raman spectra (Figure 3) with the peaks corresponding to six phonon modes between 200 $cm^{-1}$and 700 cm^{-1}. The spinel structure of ferrites show 39 vibrational modes out of which six phonon modes are Raman active ($2A_{1g}$, E_g, and $3T_{2g}$). The modes above 600 cm^{-1}correspond to metal-oxygen (M-O) (symmetrical stretching) bonding at tetrahedral sites and the modes below 600 cm^{-1} correspond to metal-oxygen bonding (symmetrical, anti-symmetrical bending) in octahedral sites.[15] As the Er concentration increases, the peaks get broadened and the peak position shifts towards higher wavelength. This shift indicates that strain is induced in the lattice due to the presence of large size Er^{+3} and the broadening is due to the smaller crystallite size.[16] Relative increase in intensities of modes corresponding to octahedral sites below 600 cm^{-1} suggests that the Er^{3+} has higher preference for octahedral sites. The red shift values are tabulated in Table I.

Figure 4 shows the magnetization (M-H) curves for Er doped cobalt-ferrites. The magnetization (M), at ~1200 kA/m, and the coercivity (H_C) values are listed in Table I. The M for $CoFe_2O_4$ is ~72 Am^2/kg. With increasing Er substitution M increases from ~72 Am^2/kg ($x = 0$) to ~75 Am^2/kg ($x = 0.02$) followed by a decrease to ~73 Am^2/kg ($x = 0.03$ and 0.04). The Er doped cobalt-ferrites ($x \le 0.02$)

TABLE I. Lattice parameter (a), average crystallite size, strain, magnetization (M), and coercivity (H_C) of $CoFe_{(2-x)}Er_xO_4$(x = 0, 0.01, 0.02, 0.03, and 0.04).

Composition	a (Å) (±0.0008)	Average crystallite size (nm)	Strain (10^{-4})	Red shift W r to X = 0.00 (cm^{-1}) (A_{1g}mode)	Mat (~1200 kA/m) Am^2/kg (±1%)	H_C (kA/m) (±1%)
$CoFe_2O_4$	8.3810	186.74	0.62	…	72.1	29.1
$CoFe_{1.99}Er_{0.01}O_4$	8.3853	135.88	0.85	18.79	72.7	60.2
$CoFe_{1.98}Er_{0.02}O_4$	8.3852	130.75	1.73	27.04	75.3	65.6
$CoFe_{1.97}Er_{0.03}O_4$	8.3847	150.98	2.38	16.73	73.3	56.2
$CoFe_{1.96}Er_{0.04}O_4$	8.3848	132.00	1.90	35.28	73.2	56.5

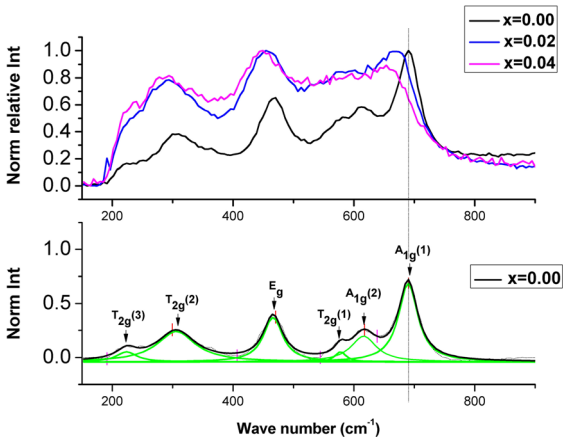

FIG. 3. Raman spectra–(upper) raw data of $CoFe_{(2-x)}Er_xO_4$ ($x = 0$, 0.02, and 0.04) and (lower) spectral analysis of $CoFe_2O_4$ as a representative, sintered at 1000 °C for 4 h.

have only marginally higher M values compared to $CoFe_2O_4$. Er^{+3} is expected to have negligible contribution to the room temperature magnetization of Er-doped cobalt-ferrites because of their low magnetic-ordering temperatures (<90 K)[17,18] and the marginal increase in M is possibly due to the rearrangement of cations in A and B sites. Because of the large ionic radii of Er^{+3} they prefer to occupy only the B site and hence disrupt the original ions distribution. Some of the Co^{+2} ions may migrate to the A site because of their large ionic radii compared to Fe^{+3} ions by replacing the equivalent amount of Fe^{+3} ions from A to B site.[18] So the net magnetization increases marginally up to $x = 0.02$. However, at higher Er content ($x = 0.03$ and 0.04) formation of antiferromagnetic $ErFeO_3$ phase leads to decrease in M. The coercivity of pure cobalt-ferrite in the current investigation is ~29 kA/m. Doping of Er ($x = 0.01$) leads to doubling (~100% increase) of H_C value (~60 kA/m) compared to undoped cobalt-ferrite. Subsequent increase in Er doping ($x = 0.02$) increases H_C value only by ~10% (~66 kA/m), followed by decrease by ~11% (~56 kA/m) for $x = 0.03$ and 0.04). Increase in H_C up to $x = 0.02$ may be due to the contribution of Er^{+3} to the anisotropy because of its strong spin orbit coupling similar to Co^{+2} ions.[18] The inset (Figure 4) shows a strong correlation between a and H_C for Er doped cobalt-ferrites. It is evident that H_C is strongly affected by lattice parameter. At lower x (0.01 and 0.02), until solubility limit, steep increase in H_C confirms sharp increase in anisotropy owing to presence of Er^{3+} in octahedral sites of the cubic spinel lattice. Marginal increase (~10%) in H_C between $x = 0.01$ and $x = 0.02$ suggests only marginal difference in the solubility among the two successive compositions owing to a steep gradient in solvus. This is corroborated with similar a values for $CoFe_{1.99}Er_{0.01}O_4$ and $CoFe_{1.98}Er_{0.02}O_4$. The presence of antiferromagnetic orthoferrite phase at higher Er compositions ($x = 0.03$ and 0.04) is expected to initiate the pinning of domain walls of the ferrimagnetic phase along with the existing increased anisotropy in the ferrimagnetic phase to control the coercivity. The domain wall motion of a ferrimagnetic phase through an antiferromagnetic phase is generally complex and in this case the two mechanisms probably work together to decreases H_C.[6]

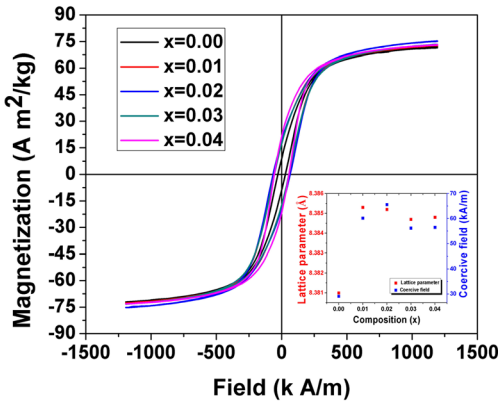

FIG. 4. Magnetization curves and (inset) correlation between lattice parameter (a) and coercive field (H_C) of $CoFe_{2-x}Er_xO_4$ ($x = 0$, 0.01, 0.02, 0.03, and 0.04) sintered at 1000 °C for 4 h.

Nanocrystalline particulates of Er doped cobalt-ferrites $CoFe_{(2-x)}Er_xO_4$ ($0 \le x \le 0.04$), were successfully synthesized using sol-gel assisted autocombustion method. Powder x-ray diffraction confirmed the formation of single phase of spinel for the compositions $x = 0$, 0.01, and 0.02 and for higher compositions ($x = 0.03$ and 0.04) an additional orthoferrite phase formed along with the spinel phase. Lattice parameter of the doped cobalt-ferrites was higher than that of pure cobalt-ferrite. The observed red shift in the doped cobalt-ferrites indicates the presence of induced strain in the cobalt-ferrite matrix due to large size of the Er^{+3} compared to Fe^{+3}. The magnetization (at ~1200 kA/m) marginally increased from ~72 Am^2/kg($x = 0$) to ~75 Am^2/kg($x = 0.02$), followed by a decrease to ~73 Am^2/kg($x = 0.03$ and 0.04).

The assistance from Dr. R. Chandrasekar (School of Chemistry, University of Hyderabad) in carrying out the Raman measurements is gratefully acknowledged. The financial and infrastructural support from University of Hyderabad is truly appreciated.

[1]Q. Song and Z. J. Zhang, J. Am. Chem. Soc. **126**, 6164 (2004).
[2]M. A. G. Soler, E. C. D. Lima *et al.*, Langmuir **23**, 9611 (2007).
[3]C. Vázquez-Vázquez *et al.*, Phys. Status Solidi A **205**, 1358 (2008).
[4]A. H. Habib *et al.*, J. Appl. Phys. **103**, 07A307 (2008).
[5]I. C. Nlebedim *et al.*, J. Appl. Phys. **113**, 193904 (2013).
[6]B. D. Cullity and C. D. Graham, *Introduction to Magnetic Materials* (Wiley/IEEE, NJ, 2009).
[7]D. J. Craik (Ed.), *Magnetic Oxides, Parts 1 and 2* (John Wiley & Sons, Bristol, 1975), Chap. 9, Pt. 2.
[8]S. R. Naik and A. V. Salker, J. Mater. Chem. **22**, 2740 (2012).
[9]T. V. Albu *et al.*, Thermochim. Acta **340–341**, 235 (1999).
[10]V. Buzko, I. Sukhno, and V. Klimova, Acta Chim. Slov. **51**, 213 (2004). Available at: http://acta.chem-soc.si/51/51-2-213.pdf.
[11]R. A. Young and D. B. Wiles, J. Appl. Crystallogr. **15**, 430 (1982).
[12]A. Goldman, *Modern Ferrite Technology*, 2nd ed. (Springer Science, Business Media Inc., 2006), Chap. 4.
[13]M. R. De Guire *et al.*, J. Appl. Phys. **65**, 3167 (1989).
[14]B. D. Cullity and S. R. Stock, *Elements of X-ray Diffraction* (Wiley, Prentice Hall, Upper Saddle River, NJ, 2001).
[15]P. Chandramohan *et al.*, J. Solid State Chem. **184**, 89 (2011).
[16]R. Nongjai *et al.*, J. Appl. Phys. **112**, 084321 (2012).
[17]B. H. Frazer, J. R. Gebhardt, and N. Ali, J. Appl. Phys. **85**(8), 6100 (1999).
[18]F. Cheng *et al.*, J. Appl. Phys. **86**(5), 2727 (1999).